JOURNAL OF THERMOPHYSICS AND HEAT TRANSFER
Vol. 21, No. 2, April–June 2007

Numerical Solution of Highly Expanded Flashing Liquid Jets

Edvaldo Angelo*
Universidade Presbiteriana Mackenzie, 01302-907 São Paulo, Brazil
and
José Roberto Simões-Moreira†
Universidade de São Paulo, 05508-900 São Paulo, Brazil

DOI: 10.2514/1.23972

Numerical simulation was carried out from a two-dimensional axisymmetric model for the expansion region of a flashing liquid jet expanding into a low-pressure environment. Typically, the flashing phenomenon is observed in laboratory experiments in which a liquid jet flows through a nozzle into a low-pressure environment, well below the saturation pressure of the liquid at the injection temperature. The present model considers that the fluid remains in the liquid phase down to the exit plane and off the nozzle, reaching high degrees of superheating or metastability, and then the metastable liquid jet undergoes a sudden phase change through an evaporation wave process. The numerical solution was carried out in two parts. In the first part, the theory of oblique evaporation waves was applied to solve the jump equations of the fast evaporation that occurs on the surface of the metastable liquid core. In the second part, the problem of the expansion region that results from the evaporation process was analyzed. This region is formed by a high-speed two-phase region and, generally, culminates with the formation of a shock wave structure enveloping the liquid core. The classical finite differences explicit method of MacCormack and a shock-capturing scheme were used, along with an accurate equation of state. Main shock wave dimensions obtained from the numerical solution were in agreement with the measured ones.

Nomenclature

A	=	nozzle exit section area
b_1, b_2	=	constant of the Lee–Kesler equation
b_3, b_4	=	constant of the Lee–Kesler equation
$C_{\beta 1}$	=	constant of the Lee–Kesler equation
C_D	=	discharge coefficient
c_1, c_2	=	constant of the Lee–Kesler equation
c_3	=	constant of the Lee–Kesler equation
d_1, d_2	=	v equation constant
h	=	specific enthalpy
h_0	=	specific total enthalpy
i, j	=	mesh index point
J	=	superficial mass flux (mass flux per unit of area)
L	=	length of metastable liquid core
M	=	Mach number
$\dot{m}$	=	mass flow rate
P	=	pressure
P_C	=	critical pressure
P_r	=	reduced pressure defined by P/P_C
R_b	=	nozzle exit section radius
R'_b	=	corrected nozzle exit section radius
r	=	cylindrical radial coordinate
r_1	=	maximum shock wave dimension (parallel to r axis)
r_2	=	maximum shock wave dimension (parallel to z axis)
s	=	specific entropy
T	=	temperature
T_C	=	critical temperature
T_r	=	reduced temperature defined by T/T_C
t	=	oblique evaporation wave tangential component velocity
V	=	fluid velocity
V_r	=	radial fluid velocity
V_z	=	axial fluid velocity
v	=	specific volume
W	=	oblique evaporation wave normal component velocity
x	=	vapor mass quality
Z	=	compressibility factor
z	=	cylindrical axial coordinate
β	=	wave angle
γ	=	Lee–Kesler equation constant
η	=	coordinate (computational plane)
θ	=	turning angle
ξ	=	coordinate (computational plane)
ρ	=	density
Φ	=	flux variable
ϖ	=	acentric factor

Subscripts

L	=	saturated liquid
V	=	saturated vapor
0	=	reservoir condition
1	=	metastable state
2	=	downstream oblique evaporation wave (Chapman–Jouguet condition)
3	=	upstream shock wave
4	=	downstream shock wave
∞	=	low-pressure chamber (backpressure)
*	=	reference state

Superscripts

av	=	average
ig	=	ideal gas property
RES	=	residual property
(r)	=	reference fluid
(0)	=	simple fluid

I. Introduction

FLASHING phenomena occur when a pressurized liquid is suddenly exposed to a low-pressure environment. There are many industrial and technological applications in which flashing has

Received 17 March 2006; revision received 11 December 2006; accepted for publication 1 January 2007.

*Professor, Escola de Engenharia, Numerical Simulation Group (GSN), Mechanical Engineering Department; eangelo@mackenzie.com.br.

†Associate Professor, Escola Politécnica, Alternative Energy Systems Laboratory (SISEA), Mechanical Engineering Department.

a fundamental and decisive presence. For example, one can mention 1) situations involving relief scenarios during an emergency blowdown of pressurized plant equipment. Safety devices like safety valves and rupture disks, for example, can at least temporarily discharge a two-phase mixture [1,2]; 2) relief lines installed for protecting pressurized vessels or reactors, located downstream from safety devices, involving several geometrical singularities such as abrupt area changes and two-phase flashing flow [3]; 3) boiling liquid expanding vapor explosions (BLEVEs). Catastrophic industrial accidents occurred in consequence of rupturing a pressurized liquefied gas storage tank [4–6], strongly tied to the energy stored in the liquid phase of a pressure vessel; 4) expansion devices flashing flows of the refrigeration cycles [7]; 5) seawater flashing desalination process [8,9]; 6) nuclear industry accidents associated with loss of coolant accidents (LOCA), rupture of pressurized water pipe, or cooling water jet discharging from a broken tube [10,11]; 7) the flashing process in some facility devices may result in a significant drop in fluid temperature and corresponding structural failure, because the temperature of the wall's component may reduce to a temperature below the ductile-brittle transition temperature of the steel from which the device is manufactured [12]; 8) separation of noble gas mixtures from petroleum in a flashing chamber [13]; 9) improvement in fuel economy and a substantial reduction in hydrocarbon emissions using flash-boiling fuel injection by diesel preheating in an engine environment [14]; 10) enhancement of the atomization producing fine and lesser drop-size sprays, potentially

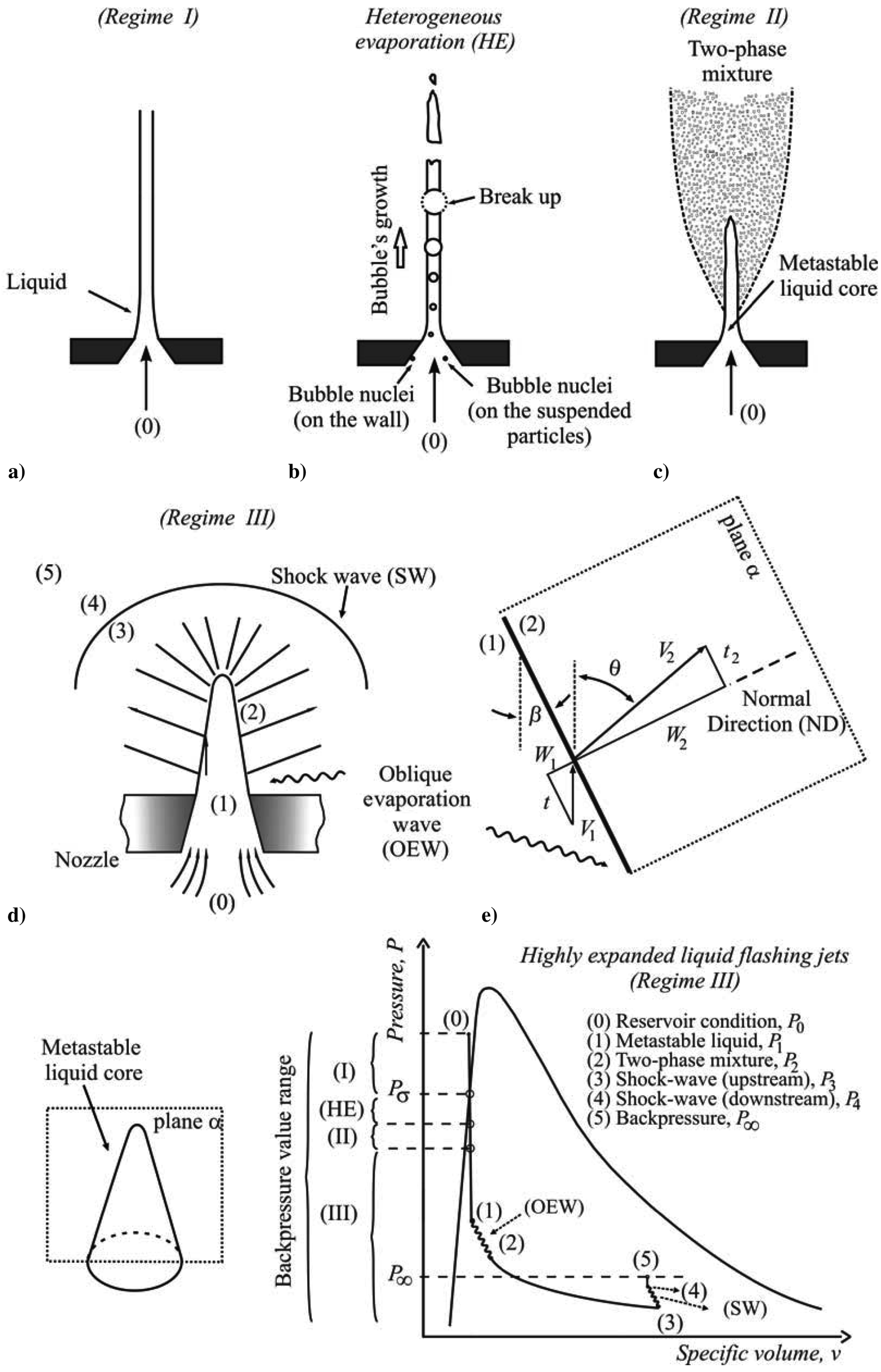

Fig. 1 Flow jet regimes: a) continuous liquid jet, regime I; b) heterogeneous nucleation phenomena; c) partially atomized liquid jet, regime II; d) highly expanded flashing liquid jet, regime III, schematic of the jet stressing the main thermodynamic states; e) schematic velocities and angles for an oblique evaporation wave; f) metastable liquid core representation; and g) pressure-specific volume plane.

useful in a wide variety of aerosol-forming processes, even of high-boiling liquids (with a small amount of low-boiling liquid propellant dissolved in the mixture [15]), among other applications.

In this way, the knowledge of relationships between the governing parameters (mainly, mass flow rate and pressure ratios) are very important to anticipate the correct flashing behavior and to furnish correct information for a proper modeling. Safety relief valves, for example, are installed in pressurized systems to ensure that the operating pressure does not exceed unsafe limits that could result in an accident [16] (tank depressurization rates depend on the mass flow crossing the valve).

The flow of saturated or nearly saturated water through orifices, nozzles, and pipes has been the periodic subject of study since 1892 [17]. Experiments with liquid substances injected in a controlled pressure chamber through a small conical convergent nozzle have shown the existence of at least three liquid jet regimes: regime I is a continuous liquid jet, regime II is partially atomized, and regime III is abrupt liquid evaporation followed by a two-phase supersonic expansion, usually terminated by shock waves (highly expanded flashing jet). Figure 1 illustrates the last regime. The first jet regime (Fig. 1a) occurs when the liquid injection process does not reach pressures equal to or below saturation pressure at injection temperature (without evaporation). Jet breakup phenomena can occur from capillary and aerodynamic instability [18]. If the pressure of the chamber (backpressure) in which the liquid is injected falls, the flow inner nozzle can accomplish pressures lower than saturation pressure and phenomena like heterogeneous evaporation can occur (Fig. 1b). Some researches [19] divide heterogeneous evaporation in two types: "wall boiling" when boiling is generated by nuclei on the nozzle wall, phenomenon practically inexistent in short nozzles, and "particle boiling" when boiling nuclei happens on particles floating within the liquid.

At lower backpressures, the liquid may achieve the superheated state. The superheated or metastable state to make oneself up by the case of the liquid reaches its boiling or saturation point without a phase transition taking place. Experiments show that the liquid jets, under moderated superheated degrees (liquid jet regime II, Fig. 1c), become intact, only to break up a certain distance after the downstream nozzle exit. Stray droplets begin to form at the surface of the jet, resulting in a diverging spray that gives rise to the spray cone angle of the jet [20,21].

At very low backpressures (liquid jet regime III, Fig. 1d), many times lower than the vapor pressure at the initial liquid temperature, a highly expanded flashing jet diverges immediately at the nozzle exit. A cloud of droplets is seen from the nozzle exit and it overshadows the vision of evaporative phenomenon. Some authors [14] assume that the spray expands like an underexpanded, choked, compressible flow and that the boiling and rapid bubble growth occurs within the nozzle, producing a two-phase, already atomized flow at the nozzle exit. Nevertheless, it is possible to conclude, by careful examination of the still pictures taken using different photographic techniques at high shutter speed, that the flow emerging from the nozzle remains in the liquid phase [22–26]. Only high-shutter-speed photographic techniques had been able to verify an intact inner-liquid-core, downstream nozzle exit section. This latter case comprises the interest in the present study.

This paper reports numerical simulation results and analyses of highly expanded flashing liquid jets. The distinction of the present study is the numerical and theoretical examination of the superheated liquid effects in the jet flow pattern. The influence of the injection liquid conditions and the backpressure values on the expansion process inner injection chamber (low-pressure chamber), as well as the main shock wave dimensions, are investigated. The mathematical model has two parts: 1) a one-dimensional model for the injection process through a nozzle that culminates in an evaporation wave downstream nozzle exit injector and 2) a two-dimensional axisymmetrical model for a two-phase flow mixture expanding in the low-pressure chamber.

The flow characteristics such as the reduced spray penetration, improved atomization, and increased spray angle found in this regime can be understood by the use of the evaporation wave theory.

Some previous researchers focused on hybrid experimental and numerical approaches to study the highly flashing liquid jets [22–25]; mainly because of the difficulties arising from the complexity of the phenomena, only one-dimensional mathematical models had been developed.

II. Highly Expanded Flashing Liquid Jet Flow Pattern

Figures 2a and 2b show a flashing liquid jet for which the images were taken using two different photographic techniques (at a high shutter speed). Figure 2a was taken using the backlighting technique, and Fig. 2b was taken using the schlieren technique. It is important to stress that both pictures were taken simultaneously.

Careful examination of a series of still pictures [25,26] similar to the ones shown in Figs. 2a and 2b allows one to conclude that the jet emerging from the nozzle remains in the liquid phase without any perceptible internal nucleation and that a cloud of droplets and shock wave structure enveloping the liquid core appear.

Images also reveal that the liquid jet exiting the nozzle forms a metastable liquid core, seen in Fig. 2a as a shining area and in Fig. 2b as a dark region. Regular still pictures cannot show physical details of some intriguing phenomena associated with flashing liquid jets, such as a shock wave structure and the liquid core. Finally, experimental results [25,26] have also indicated that the mass flow rate is upper-limited, displaying a chocking behavior.

Evidently, the occurrence of the metastable liquid core, a shattering jet (a cloud of droplets), and shock wave structure enveloping the liquid core depend on several factors, including the thermodynamic properties of the substance, the degree of superheating, the absence of activated nucleation sites, and the depressurization time scale. Many experimental tests had used isooctane due to its high degree of evaporation reached during a liquid flashing process [24–26]. This fact is also capable of explaining the reasons why some researchers [18,27], had not obtained high degrees of evaporation and patterns like the one described before (using water as the test substance, for example). Even the addition of a lighter component in the principal substance can cause nucleation, vapor bubble growth, and a complete change in the evaporation dynamics [15].

The concept of metastable liquid flow is not new and was introduced by Silver and Mitchell [28], who considered that the flow through a nozzle could be pictured as a metastable liquid core surrounded by a vapor annulus. A finite disturbance would cause the

a)

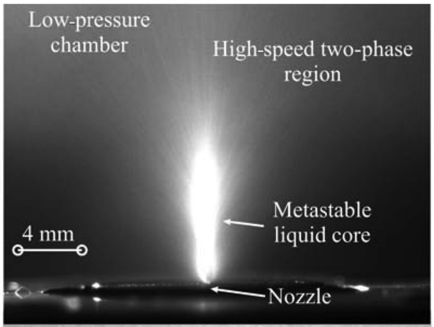

b)

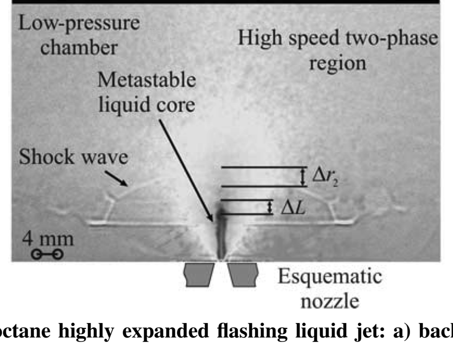

Fig. 2 Isooctane highly expanded flashing liquid jet: a) backlighting photography technique and b) schlieren photography technique; $P_0 = 500$ kPa, $T_0 = 76^\circ$C, and $P_\infty = 0, 11$ kPa.

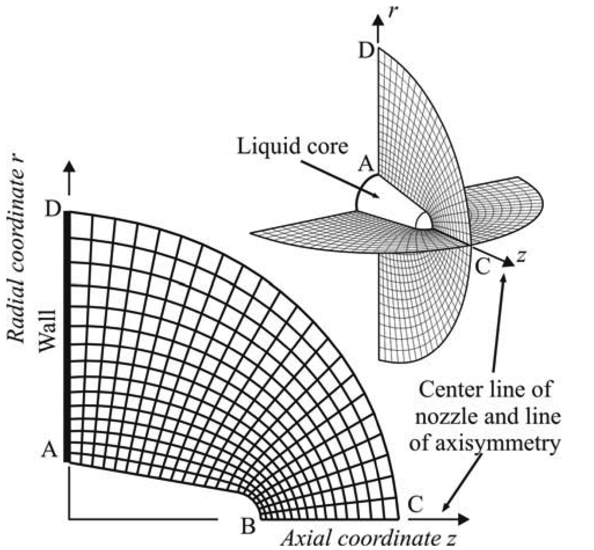

Fig. 3 Grid representations of the three-dimensional and physical planes.

metastable state to revert to a more stable state [29]. Other authors have also verified the presence of a liquid core in orifices and expansion devices in experiments at similar thermodynamic conditions [3,7].

The authors have proposed [25] a physical description of flashing liquid jets to explain the chocking behavior and the presence of shock waves. The pictorial diagram in Fig. 1d summarizes the significant details of the flashing process studied in this paper. Relevant thermodynamic states at the main points of the flashing process are pointed out in the pressure-specific volume plane in Fig. 1f.

According to the present analysis, flashing takes place on the surface of the liquid core through an evaporation wave process ($1 \rightarrow 2$), which usually produces a sonic two-phase flow, but can also be subsonic in less severe conditions (higher backpressure). This sonic state 2 is also a point of maximum mass flow rate given by the Chapman–Jouguet condition. Next, the freshly sonic two-phase flow expands to a high supersonic flow ($2 \rightarrow 3$), to eventually terminate the supersonic expansion process throughout a shock wave structure ($3 \rightarrow 4$), to finally subsonically compress the fluid up to the pressure chamber ($4 \rightarrow 5$) in the far field.

With the usual assumption of incompressible flow, the simplified version of Bernoulli's equation applied between the injection state 0 and the nozzle exit plane 1, along with the measured mass flow rate, imply that the emerging liquid must be highly superheated or metastable at the nozzle exit section, that is, the liquid state has entered deeply into the metastable region.

III. Estimation of the Thermodynamic State of the Metastable Liquid Core

Thermodynamic conditions of flow in the nozzle exit cannot be directly measured by the usual laboratory instrumentation. However, it can be inferred from mass flow rate and injection pressure measurements. In accordance, the exit metastable pressure is given by the following expression:

$$P_1 = P_0 - \frac{\dot{m}^2 v_1}{2A^2 C_D^2} \tag{1}$$

The previous equation is the energy conservation law applied to a streamline from the reservoir stagnant condition 0 to the nozzle section exit 1. The temperature of state 1 was approximated by the injection temperature value, assuming an isothermal process between [30] the state 0 and the state 1, thus $T_1 \approx T_0$. With the pair of properties T_1 and P_1 and an equation of state, one may calculate the remaining thermodynamic properties. The thermodynamic properties are considered uniform and constant within the metastable liquid core and equal to the one at the nozzle exit plane (T_1).

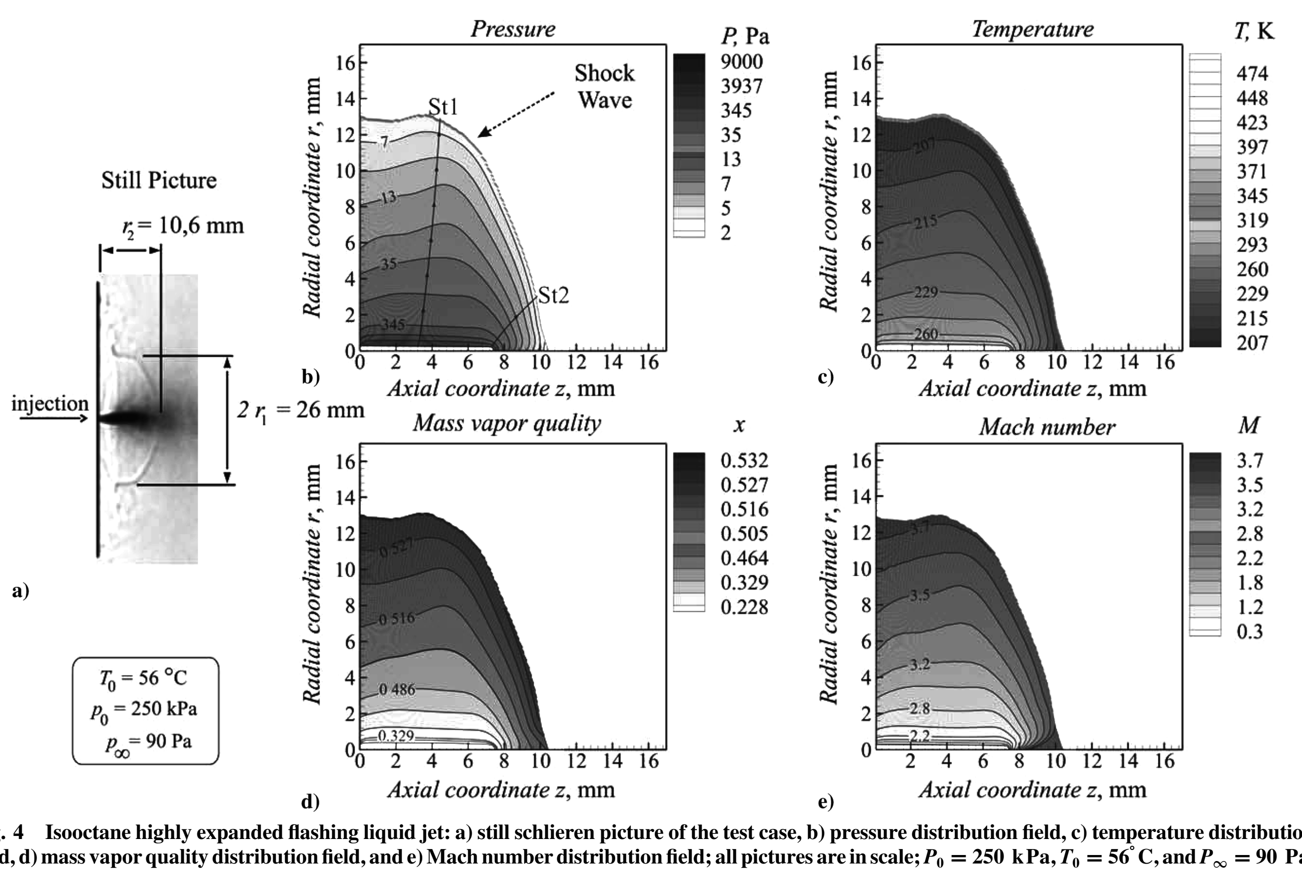

Fig. 4 Isooctane highly expanded flashing liquid jet: a) still schlieren picture of the test case, b) pressure distribution field, c) temperature distribution field, d) mass vapor quality distribution field, and e) Mach number distribution field; all pictures are in scale; $P_0 = 250$ kPa, $T_0 = 56^\circ$C, and $P_\infty = 90$ Pa.

Table 1 Numerical results

Series		Metastable state										C–J condition						SW dimensions or figure number [d]			
																		Experiments		Simulation	
P_0, kPa	T_0, °C	P_0, kPa	T_0, °C	P_∞, kPa	$\dot{m}$, g/s	L, mm	C_D	P_1, kPa	ν_1, m^3/kg	β, deg	θ, deg	P_2, kPa	T_2, °C	x_2, %	ν_2, m^3/kg	W_2, m/s	R'_b, mm	r_1, mm	r_2, mm	r_1, mm	r_2, mm
125[a]	56	122.1	56.4	Fig.[d]	0.845	6.9	0.9124	6.175	0.00151	0.2	76.36	3.412	11.847	28.467	1.8466	71.458	0.485	8a	8b	8a	8b
	76	122.7	75.2	ns[e]	0.834	5.2	0.9165	7.743	0.00155	0.21	78.5	4.1559	15.274	38.898	2.0949	86.728	0.449	ns[e]	ns[e]	ns[e]	ns[e]
	95	123.5	94.8	ns[e]	0.802	3.1	0.9195	14.71	0.0016	0.38	80.05	7.3981	27.479	45.039	1.4134	101.74	0.518	ns[e]	ns[e]	ns[e]	ns[e]
250[a]	56	250.2	56.5	Fig.[d]	1.217	7.2	0.9216	14.39	0.00151	0.39	62.4	9.1018	31.806	16.473	0.4316	47.854	0.261	7a[d]	7b[d]	7a e 9a[d]	7b e 9b[d]
	76	251.5	76.7	Fig.[d]	1.218	6	0.94	17.88	0.00155	0.38	69.71	10.402	34.533	28.5	0.6523	69.925	0.268	ns[e]	ns[e]	ns[e]	ns[e]
	95	251.3	95.5	ns[e]	1.635	6.3	0.9339	64.97	0.0016	1.17	53.8	42.952	71.437	17.88	0.1114	49.889	0.188	ns[e]	ns[e]	ns[e]	ns[e]
500[a]	56	501.6	56.6	Fig.[d]	1.746	11	0.9288	23.23	0.00151	0.62	24.88	19.076	49.348	5.081	0.0667	16.846	0.159	8c[d]	8d[d]	8c e 9a[d]	8d e 9b[d]
	76	496.3	76.7	ns[e]	1.695	7.5	0.9319	35.69	0.00155	0.67	58.85	20.003	50.417	18.271	0.2272	59.921	0.179	ns[e]	ns[e]	ns[e]	ns[e]
	95	503.4	95.4	ns[e]	1.635	6.3	0.9339	64.97	0.0016	1.17	53.8	42.952	71.437	17.88	0.1114	49.889	0.188	ns[e]	ns[e]	ns[e]	ns[e]
750[a]	56	751.1	56.4	Fig.[d]	2.161	14.1	0.933	25.83	0.00151	0.67	20.297	20.38	50.747	3.962	0.0498	16.73	0.170	8e[d]	8f[d]	8e, 9a, 11a[d]	8f, 9b, 11b[d]
	76	752.5	77	Fig.[d]	2.091	10.2	0.926	42.67	0.00156	0.64	31.95	34.135	62.322	10.699	0.089	27.815	0.161	10a[d]	10b[d]	10a, 11a[d]	10b, 11b[d]
	95	752.3	96.4	Fig.[d]	2.029	7.3	0.9374	80.97	0.0016	1.35	36.43	60.126	81.696	11.332	0.0527	33.681	0.154	10c[d]	10d[d]	10c, 11a[d]	10c, 11d[d]
2400[b]		2397	204	5.73	21.4	9[f]	0.830[f]	450.5	0.00201	2.53	55.91	263.29	136.81	67.143	0.0741	119.49	0.433	12.5	15	8.9	10
	200	2338	200	8.25	21.5	9[f]	0.838[f]	435.9	0.00198	2.5	55.23	256.94	135.67	63.745	0.0721	115.25	0.434	7	11	6.7	9.8
		2293	200	9.87	21.4	9[f]	0.843[f]	430.8	0.00198	2.47	55.9	250.72	134.58	64.488	0.0746	117.6	0.435	6.5	12	6.3	
1500[c]	20	1500	20	1	6.85	12[f]	0.95[f]	10.9	0.00053	0.13	34.07	6.687	−3.8	15.854	0.1555	25.656	0.543	15.75	ni[g]	16.4	15.7

[a] Vieira [26], with isooctane (C8H18) fluid test and nozzle exit radius 0.154 mm.
[b] Athans [24], with isooctane (C8H18) fluid test and nozzle exit radius 0.432 mm.
[c] Kurschat et al. [23], with C6F14 fluid test and nozzle exit radius 0.18 mm.
[d] Number of the corresponding figure.
[e] Not shown (see Angelo [30]).
[f] Estimated.
[g] Not informed by Athans [24].

IV. Oblique Evaporation Wave Jump

The oblique evaporation is a phase-change discontinuity similar to deflagration waves in a combustion gas. To calculate jump properties across the metastable liquid two-phase interface, the mass, momentum, and energy conservation equations must be solved. Assuming uniform thermodynamic properties within a phase domain, the downstream state 2 is at a thermodynamic equilibrium (thermal and mechanical) and that the process is at steady state, then the 1-D mass, momentum, and energy conservation equations [30,31] are, respectively,

$$[J] = 0 \tag{2}$$

$$[P + WJ] = 0 \tag{3}$$

$$[h + W^2/2] = 0 \tag{4}$$

The square brackets indicate a jump in the enclosed value, that is, $[f] = f_2 - f_1$. For a given metastable liquid upstream state 1, there exists a corresponding singular solution for low downstream pressure values (state 2). This solution is the Chapman–Jouguet (C–J) condition. In the C–J solution, the two-phase normal velocity W_2 is sonic. Behind the oblique evaporation wave, the flow is deflected by the flow-turning angle (see Fig. 1e), and the wave angle can be found according to [30]

$$\sin\beta = \frac{\pi W_2 R_b^2}{v_2 \dot{m}} \tag{5}$$

Evidently, the mass flow rate crossing the nozzle exit plane must also cross the oblique evaporation wave. In this way, the metastable liquid core should take a conical shape. It is possible to relate the turning angle, the wave angle, and the specific volumes downstream and upstream of the evaporation wave with an expression proceeding from the manipulation of trigonometric [30,31] relations and mass conservation:

$$tg\theta = \frac{\sin(2\beta)}{2(\sin^2\beta + \frac{1}{v_2/v_1 - 1})} \tag{6}$$

State 2 is completely determined. To obtain all thermodynamic properties, a realistic equation of state has been used (the cubic equation of state of Lee and Kesler [32]).

V. Expansion Region and Shock Wave Position

After the sudden evaporation ($1 \rightarrow 2$) through an oblique evaporation wave, the two-phase mixture continues to expand further. Pressure, temperature, and density fall substantially during the expansion process and the velocity and the Mach number increase, reaching high supersonic values and giving rise to a strong shock wave formation located at some distance from the nozzle exit enveloping the whole flashing liquid. The simulation considered a series of simplifying assumptions used throughout the formulation of the model for the two-phase flow, among which were no gravitational effects, no effects of surface tension, inviscid flow, and a homogeneous two-phase flow model.

The two-dimensional axisymmetric model used a cylindrical coordinate system (z, r), where the coordinate z coincides with the nozzle centerline, and r is the distance from the centerline.

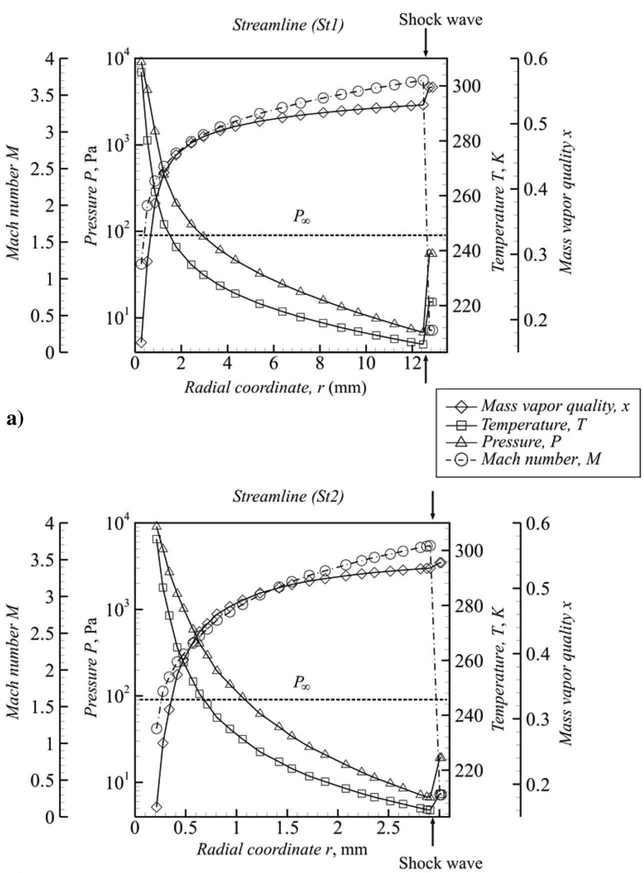

Fig. 5 Mass vapor quality, temperature, pressure, and Mach number for the streamlines St1 and St2 (see Fig. 4a).

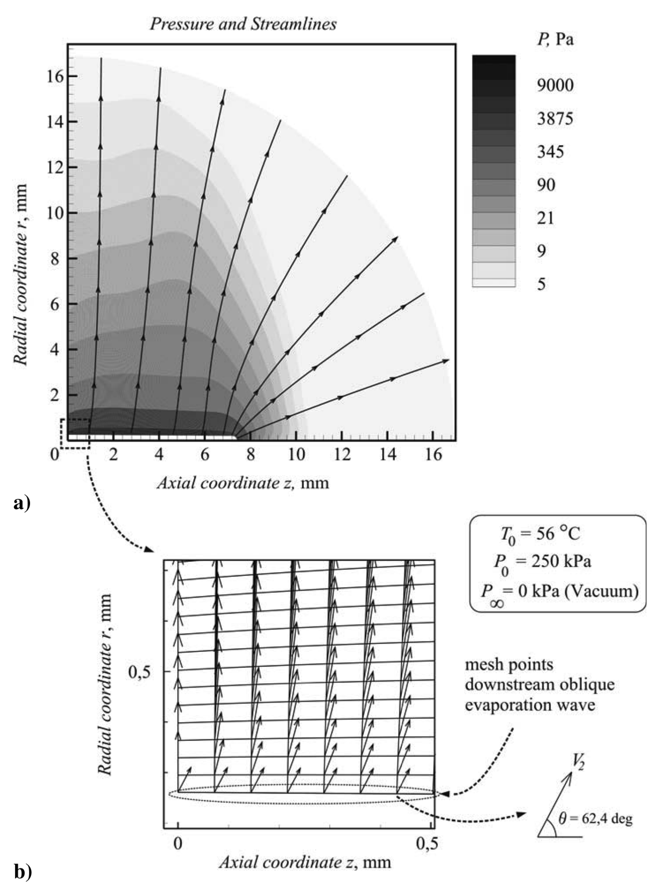

Fig. 6 Isooctane highly expanded flashing liquid jet: a) pressure distribution field and some streamlines and b) detail of some vector velocities near the metastable liquid core; $P_0 = 250$ kPa, $T_0 = 56^\circ$C, and $P_\infty = 0$ kPa (vacuum).

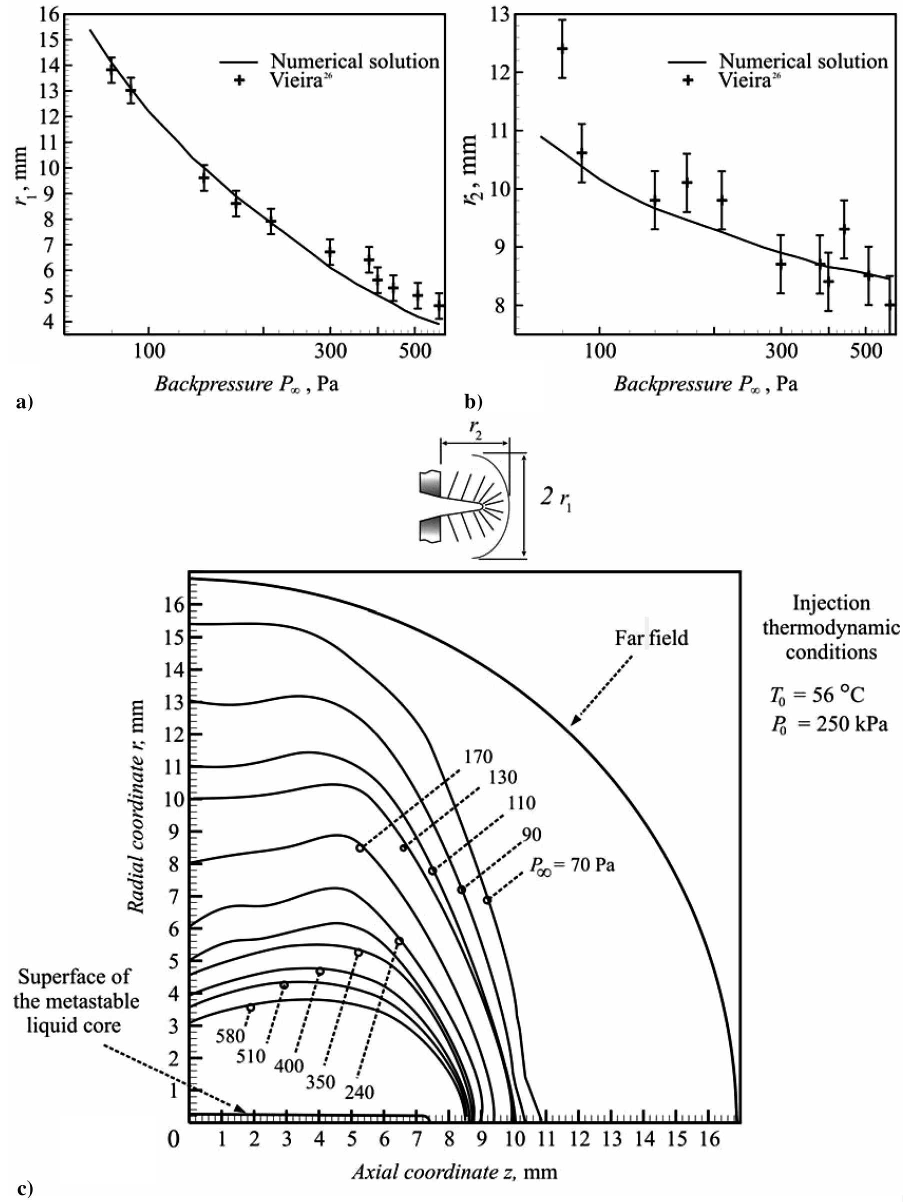

Fig. 7 Isooctane highly expanded flashing liquid jet: a) maximum shock wave dimension in radial direction vs backpressure, experimental and numerical simulation results; b) shock wave maximum dimension in axial direction vs backpressure, experimental and numerical simulation results; and c) shock wave shape with backpressure variation (with constant injection pressure and temperature); $P_0 = 250$ kPa and $T_0 = 56^\circ$C.

A. Mesh

The expansion region of the two-phase flow is discretized using an elliptic grid generation procedure. It is known that the systems of elliptic second-order partial differential equations produce the best possible grids in the sense of smoothness and grid point distribution [33]. Figure 3 shows the mesh in the physical plane and its three-dimensional view.

To prevent incompatibility with the axisymmetric model and numerical instabilities, the conical metastable liquid core has its extremity rounded off (see Fig. 3). Extinction lengths of the metastable liquid core are obtained from still photographic records, as indicated in [26].

The correspondence between the limits of the physical plane and the nondimensional computational plane (a rectangular mesh, with axis ξ and η) is line AB $\rightarrow \xi = 0$, line DC $\rightarrow \xi = 1$, line BC $\rightarrow \eta = 0$, and line AD $\rightarrow \eta = 1$.

B. System of Conservation Equations and Thermodynamic Properties Determination

Standard procedure requires that the set of independent variables in the physical plane (z, r) must be transformed into a new set of independent variables in the transformed computational rectangular grid space (ξ, η), that is, a computational rectangular grid. The general system of equations is

$$\frac{\partial \Phi}{\partial \xi} = B - \frac{\partial G}{\partial \eta}\frac{\partial \eta}{\partial r} - \frac{\partial F}{\partial \eta}\frac{\partial \eta}{\partial z} \tag{7}$$

$$\Phi = \begin{bmatrix} \rho\left(V_z \frac{\partial \xi}{\partial z} + V_r \frac{\partial \xi}{\partial r}\right) \\ (\rho V_z^2 + p)\frac{\partial \xi}{\partial z} + (\rho V_r V_z)\frac{\partial \xi}{\partial r} \\ (\rho V_z V_r)\frac{\partial \xi}{\partial z} + (\rho V_r^2 + p)\frac{\partial \xi}{\partial r} \\ (\rho h_0 + p)\left(V_z \frac{\partial \xi}{\partial z} + V_r \frac{\partial \xi}{\partial r}\right) \end{bmatrix} \tag{8}$$

$$B = \frac{\rho}{r}\begin{bmatrix} V_r \\ V_r V_z \\ \rho V_r^2 \\ V_r h_0 \end{bmatrix} \tag{9}$$

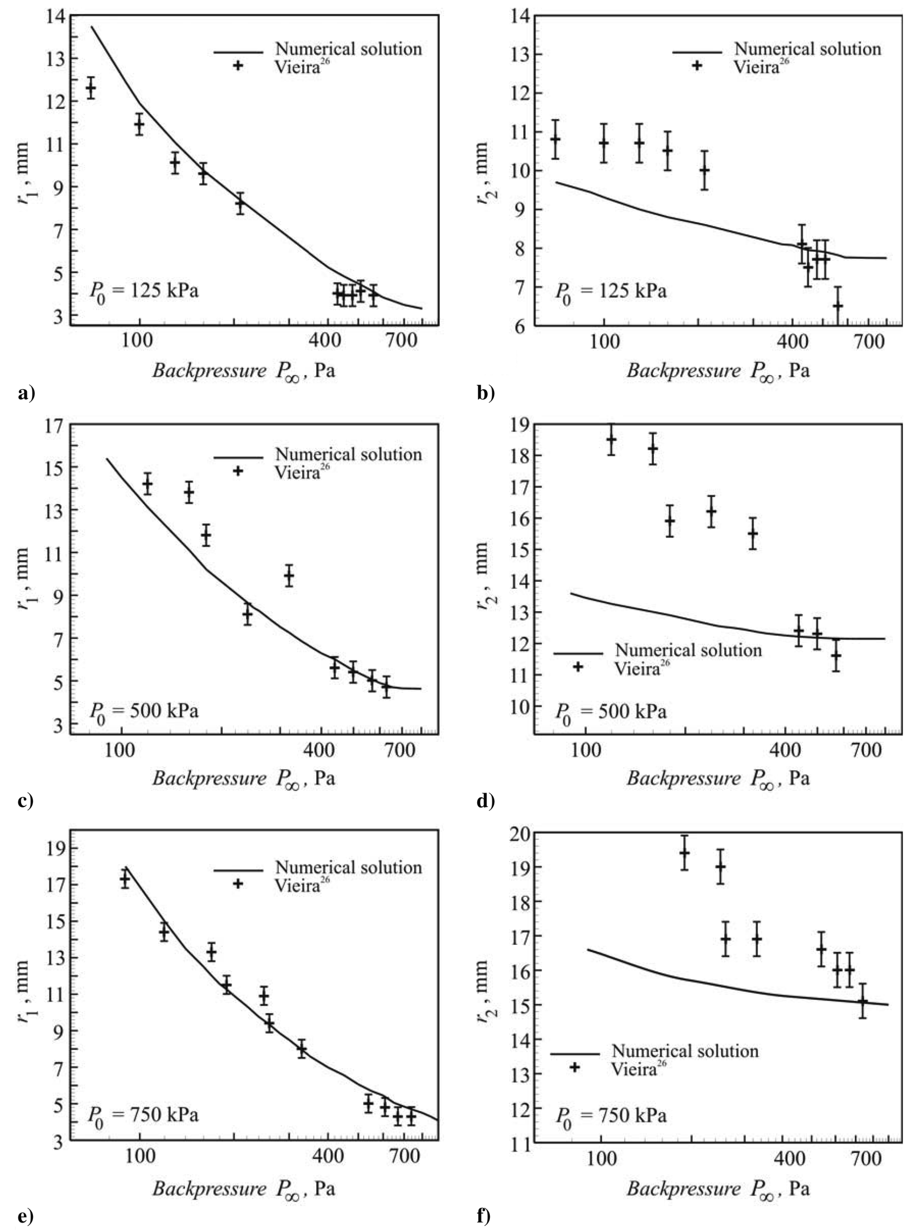

Fig. 8 Shock wave maximum characteristic dimensions vs backpressure, experimental, and numerical simulation results: a) $P_0 = 125$ kPa, b) $P_0 = 125$ kPa, c) $P_0 = 500$ kPa, d) $P_0 = 500$ kPa, e) $P_0 = 750$ kPa, and f) $P_0 = 750$ kPa; isooctane with $T_0 = 56^\circ$C for all cases.

$$G = \begin{bmatrix} \rho V_r \\ \rho V_r V_z \\ \rho V_r^2 + p \\ \rho V_r h_0 \end{bmatrix} \tag{10}$$

$$F = \begin{bmatrix} \rho V_z \\ \rho V_z^2 + p \\ \rho V_r V_z \\ \rho V_z h_0 \end{bmatrix} \tag{11}$$

The system of conservation equations formed by Eqs. (7–11) is hyperbolic when applied to a two-dimensional supersonic flow [29]. The thermodynamic properties determination uses a Lee–Kesler [32] equation of state:

$$Z = \frac{P_r v_r'}{T_r} = 1 + \frac{C_B}{v_r'} + \frac{C_C}{v_r'^2} + \frac{C_D}{v_r'^5} + \frac{c_4}{T_r^3 v_r'^2}\left(C_{\beta 1} + \frac{\gamma}{v_r'^2}\right)\exp\left(-\frac{\gamma}{v_r'^2}\right) \tag{12}$$

$$C_B = b_1 - \frac{b_2}{T_r} - \frac{b_3}{T_r^2} - \frac{b_4}{T_r^3} \tag{13}$$

$$C_C = c_1 - \frac{c_2}{T_r} + \frac{c_3}{T_r^3} \tag{14}$$

$$C_D = d_1 + \frac{d_2}{T_r} \tag{15}$$

$$v_r' = \frac{v P_C}{R T_C} = \frac{P_C}{\rho R T_C} \tag{16}$$

$$Z = Z^{(0)} + \frac{\varpi}{\varpi^{(r)}}\left(Z^{(r)} - Z^{(0)}\right) \tag{17}$$

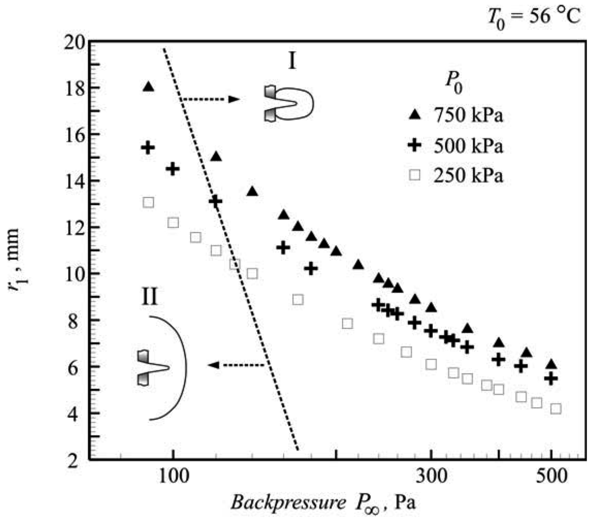

a)

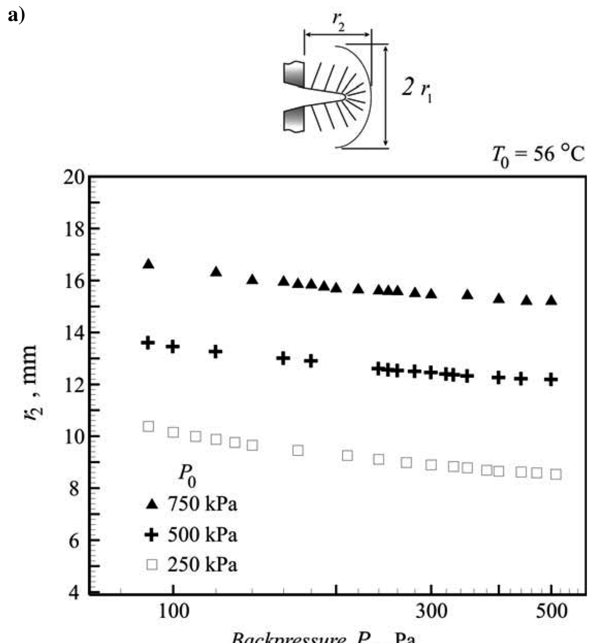

b)

Fig. 9 Influence of shock wave maximum dimensions with injection pressure variation; numerical simulation results: a) r_1 vs backpressure and b) r_2 vs backpressure; isooctane with $T_0 = 56^\circ$C for all cases.

The substance interest compressibility factor is related by Eq. (17) with the compressibility factor and the acentric factor of a simple fluid and a reference fluid. All constants in Eqs. (12–15) are tabled to the simple fluid and the reference fluid, as well as to the acentric factor. The solution sequence that assumes the preestablished pair of temperature and pressure is to

1) Obtain the compressibility factor for the simple fluid using Eqs. (12–16) and simple fluid tabled constants.

2) Obtain the compressibility factor for the reference fluid using the same Eqs. (12–16) and reference fluid tabled constants.

3) Determine the substance interest compressibility factor with Eq. (17). and

4) Determine the specific volume using Eqs. (12) and (15). The specific enthalpy could be estimated using the residual properties technique:

$$\frac{h^{\mathrm{RES}} - h_*}{RT_c} = T_r\left[Z^{(0)} - 1 - \frac{b_2 + 2b_3/T_r + 3b_4/T_r^2}{T_r(\nu_r')} - \frac{c_2 - 3c_3/T_r^2}{2T_r(\nu_r')^2} + \frac{d_2}{5T_r(\nu_r')^5} + 3E\right] \tag{18}$$

$$E = \frac{c_4}{2T_r^3\gamma}\left\{C_{\beta 1} + 1 - \left[C_{\beta 1} + 1 + \frac{\gamma}{(\nu_r')^2}\right]\exp\left[-\frac{\gamma}{(\nu_r')^2}\right]\right\} \tag{19}$$

$$\left(\frac{h^{\mathrm{RES}} - h_*}{RT_C}\right) = \left(\frac{h - h_*}{RT_C}\right)^{(0)} + \frac{\varpi}{\varpi^{(r)}}\left[\left(\frac{h^{\mathrm{RES}} - h_*}{RT_C}\right)^{(r)} - \left(\frac{h^{\mathrm{RES}} - h_*}{RT_C}\right)^{(0)}\right] \tag{20}$$

The determination of the specific enthalpy is similar to that employed in the determination of specific volume:

1) Obtain the difference between specific residual enthalpy and simple fluid with Eqs. (18) and (19).

2) Repeat the last procedure to the reference fluid.

3) Determine the specific residual enthalpy to the interest substance. The specific enthalpy is obtained by

$$h = h^{\mathrm{RES}} + h^{\mathrm{ig}} \tag{21}$$

If the two-phase thermodynamic condition is reached, a mixture law should be used:

$$v = xv_V + (1 - x)v_L \tag{22}$$

$$h = xh_V + (1 - x)h_L \tag{23}$$

C. Numerical Method

The system of conservation equations is solved using the classical MacCormack's integration technique, which is an explicit finite difference technique of second-order accuracy.

The flowfield can be computed by starting with a given initial data line that corresponds to the downstream oblique evaporation wave (state 2 in Figs. 1d, 1e, and 1g), for which the magnitudes and properties (P, T, ρ, V_r, and V_z) had been determined by solving the jump equations (2–4) and then solving the system of conservation equations (7–11) numerically, marching down step by step [30]. A flux variable Φ is obtained for the next step $i + 1$, using the following expression:

$$\Phi_{i+1,j} = \Phi_{i,j} + \left(\frac{\partial \Phi}{\partial \xi}\right)_{\mathrm{av}}(\mathrm{d}\xi) \tag{24}$$

The ξ derivative of Φ, a representative average value between $\xi + \Delta\xi$, can be found from Eq. (7) by means of a predictor-corrector approach. In the predictor step, the η derivative in Eq. (7) is replaced by forward differences, and in the corrector step, it is replaced by rearward differences.

After the prediction-corrector steps, it is necessary to obtain the primitive variables (temperature, pressure, mass vapor quality, radial velocity, and axial velocity) by decoding the flux variables. The decoding process is the most complex stage of the numerical procedure. First, it is quite time-consuming to solve a realistic equation of state as it has been carried out in the present work [Eqs. (12–17) and (20) and additional equations to determine other thermodynamic properties, Eqs. (18–21) and (23)], mainly because the thermodynamic equation of state and the other thermodynamic relations are not in the canonic form. Second, the two-phase flow expansion of a hydrocarbon such as isooctane can result in a complete evaporation process [23,34]. Third, it is necessary to solve a system of nonlinear equations. In similar supersonic aerodynamic problems in which the perfect gas hypothesis is assumed as being true everywhere, the decoding stage is direct and simple.

In association with MacCormack's method, a shock-capturing scheme was also implemented in which oblique shock waves are located between the points of the mesh and the jump equations [30]

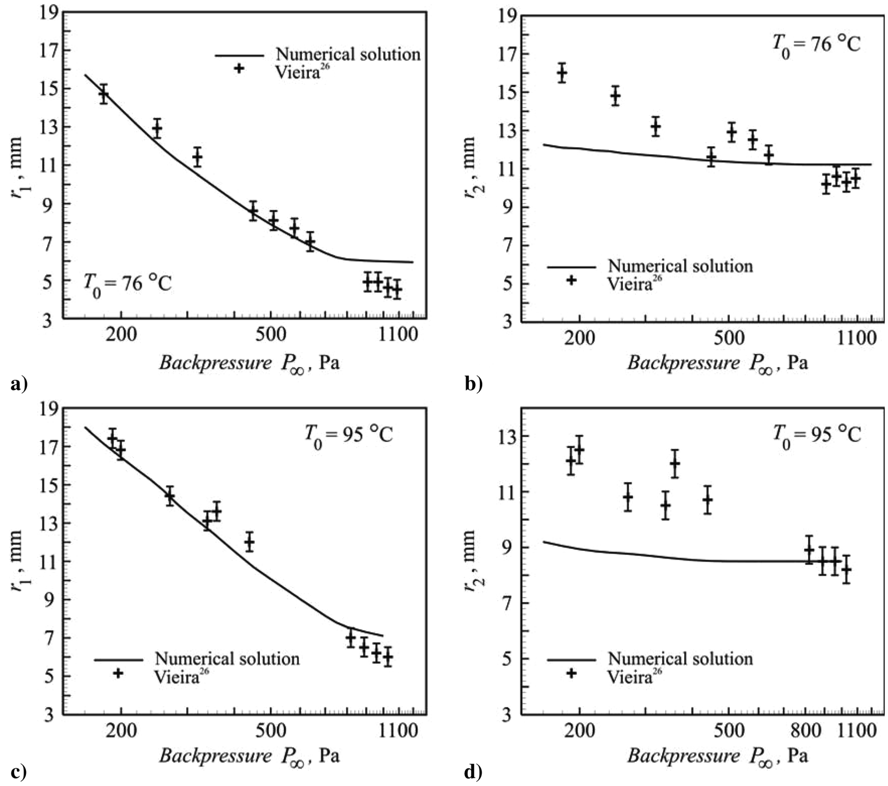

Fig. 10 Shock wave maximum characteristic dimensions vs backpressure, experimental, and numerical simulation results: a) $T_0 = 76^\circ$C, b) $T_0 = 76^\circ$C, c) $T_0 = 95^\circ$C, and d) $T_0 = 95^\circ$C; isooctane with $P_0 = 750$ kPa for all cases.

are verified; if they are not satisfied at that specific location, the shock position is moved to the next grid points downstream.

D. Boundary Conditions

Because of the inviscid flow hypothesis, the flow is tangent to the base wall (points of mesh where $z = 0$). In all points in the axisymmetry line ($r = 0$), the radial velocity vanishes. At each step, the direction of the velocity vector of the points located along the wall are corrected so that they are always parallel to it. The backpressure is also a boundary condition, as well as a sonic condition, after an evaporation wave.

VI. Numerical Solution Procedure

The solution procedure is described as follows:

1) Discharge coefficient, mass flow rate, length of the metastable liquid core (extinction length), and initial conditions (injection pressure and temperature) are furnished as input data. The metastable pressure P_1 is calculated from Eq. (1). It is also assumed that the liquid injection temperature T_0 is kept constant and that the specific volume is equal to the saturation value at T_0 down to the nozzle exit section.

2) The jump equations are solved [Eqs. (2–4)] by assuming the singular C–J solution.

3) The wave angle and the deflection angle θ are calculated next, according to Eqs. (5) and (6), respectively. The radius of the base R_b of the metastable liquid core is corrected (R'_b), taking into consideration the superficial mass flow of the liquid core.

4) The expansion field is obtained using MacCormack's method. At the same time, the position of the shock wave is obtained by using the shock-capturing scheme.

VII. Results of Numerical Solution

Table 1 presents relevant results of the numerical solution compared with experimental conditions reported in literature [23,24,26]. The first and second columns display the experimental nominal values for temperature and pressure condition injection. The next three columns present the main experimental conditions, which are the injection pressure P_0, the injection temperature T_0, and the reservoir pressure or backpressure P_∞. The mass flow rate, the length of metastable liquid core, and the discharge coefficient accomplish the reported literature's necessary data for the numerical simulation. The metastable condition P_1 is also shown. With regard to Table 1, the set of columns labeled "C–J condition" refer to the downstream states of the one-dimensional solution of the evaporation wave. The last three columns present the correct nozzle diameter R'_b and the main dimensions of the shock waves (r_1 and r_2).

Grayscale of the expansion field after the shock waves shown in Figs. 4b–4e is not part of the solution and it has been plotted only to emphasize relevant points (the numerical solution is carried out up to the shock wave only). Figures 5a and 5b show the field of distribution of some properties for two streamlines (St1 and St2) drawn in Fig. 4b.

Figure 5 shows four different graphs (mass vapor quality, temperature, pressure, and Mach number), stressing property variation of the two-phase mixture downstream of the oblique evaporation wave to the chosen streamline (St1 and St2) as a function of the radial position. The results indicate that starting at the sonic two-phase flow (at the C–J condition and pressure P_2), the mixture expands to increasing Mach numbers, whereas the pressure decreases to values well below the low-pressure chamber just a few millimeters down the evaporation wave. The supersonic expansion terminates with a shock wave, which increases the pressure to P_4, and finally, the fluid is compressed (at subsonic velocities) to the low-pressure chamber P_∞ in the far field (this last process is not shown in Fig. 5).

The study indicates that the main flow velocity undergoes a drastic change in direction. Originally, the flow was in the axial direction; as it goes through evaporation in the interfacial region, it turns away from the interface and spreads out, which is quite consistent with the still experimental pictures [23–26].

Isooctane is a substance for which the behavior is described in the literature as retrograde [30], which means that a high degree of evaporation can be reached during a liquid flashing process. This fact can easily be verified in this study by analyzing the high mass vapor quality reached (Figs. 4d, 5a, and 5b). Many researchers [22–26], aiming to attain the clearest photograph registers, have used retrograde behavior substances such as isooctane.

Comparing the still picture (Fig. 4a) to the corresponding simulation result, one can notice that the main dimensions of the shock wave agree quite well with the numerical model, which corroborates some of the assumptions made here. A preliminary model developed by the authors [25] had considered a one-dimensional model capable of anticipating only the order of magnitude of the location of the shock wave. In that case, the shock wave was considered as having a hemispheric shape, and the value of the position of the shock wave occurred at the radius 31 mm. Other authors [24] developed a different one-dimensional model, obtaining answers with lesser accuracy (using other experimental conditions).

If the expansion process occurs at the same injection thermodynamic conditions shown in Fig. 4, however, in a nearly vacuum chamber ($P_\infty = 0$), Fig. 6a illustrates the pressure distribution and some streamlines, and Fig. 6b shows a detail of vector direction velocity variation near the metastable liquid core. The streamlines emphasize one of the characteristics of highly expanded flashing jets observed in photographic documentation [23,24,26]: the almost 90-deg flow-direction change (related to the liquid direction injection) immediately following the nozzle exit.

A. Influence of Backpressure on Shock Wave Position

For a given injection pressure and temperature, still pictures and the numerical simulation indicated that the shock wave size increases with decreasing the backpressure. This finding also means that each time, the location at which the shock wave structure is formed is farther away from the nozzle exit as the backpressure is lowered, which can clearly be seen in Fig. 7. Consequently, the representative lengths r_1 and r_2 decrease with increasing the backpressure.

The mathematical model seems to foresee with more precision, when confronted with the experiments, the maximum shock wave dimension in the radial direction (r_1) than in the axial direction (r_2). The maximum shock wave dimension in the axial direction (r_2) is less sensitive to the backpressure variations, when compared with the maximum shock wave dimension in radial direction variations (r_1).

The maximum shock wave dimension in the axial direction (r_2), in all the numerical tests carried out, shows to be much more sensitive to the length of the metastable liquid core input than to any other variable (a fact that does not occur with the r_1 dimension). The errors in the determination of the metastable liquid core length by way of the photographic measurements have probably seriously influenced the model results for the r_2 dimension. A cloud of droplets makes it very difficult to accurately know exactly where the metastable liquid core ends. Figure 2b illustrates the uncertainties in the measurements of metastable liquid core length dimension L (ΔL dimension). This cloud of droplets also confuses the determination of the r_2 dimension (see Δr_2 in Fig. 2b).

B. Influence of Injection Pressure on Shock Wave Position

Analysis of the graphics in Figs. 8 and 9 allows the conclusion that by increasing the injection pressure (keeping the backpressure constant), the length r_1 and r_2 tend to also increase. A curiosity can be observed in Fig. 9: the shift of cylindrical structure shape shock wave for a flattened shape shock wave. In Fig. 9, a hatched line indicates the point at which the maximum length shock wave dimensions are equal in both directions.

The explanation for the maximum shock wave dimension increases when the injection increases is the major upstream evaporation pressure (C–J condition pressure; see Table 1). Thus, the two-phase flow must cover a bigger space during the expansion, to reach the necessary expansion for the shock wave formation.

C. Influence of Injection Temperature on Shock Wave Position

Analysis of the graphics in Figs. 10 and 11 allows the conclusion that by increasing the test temperature, the length r_1 slightly increases, but r_2 tends to decrease. Higher injection temperature even produces major C–J pressures; however, only the r_1 shock wave dimension increases, producing an apparent paradox that is evidently explained by the analysis of the metastable liquid core length behavior. The experiments [24–26] show the metastable liquid core length decreases with increases of injection temperature; this decrease effect supplants the increased C–J pressure effect on the shock wave dimension r_2.

VIII. Limitations and Observations About the Model and the Phenomenon

The model presented for the highly expanded flashing liquid jets has limitations due to assumptions and approximations in the mathematical representation of the physical problem. The main limitations are as follows:

1) An extensive analysis of the experimental results presented in the literature was nonconclusive about a simple correlation of the metastable liquid degree reached during liquid nozzle flow and the main flow conditions. Thus, the metastable state for the liquid in the nozzle exit is unknown, imposing its indirect determination by measuring of flow mass rate.

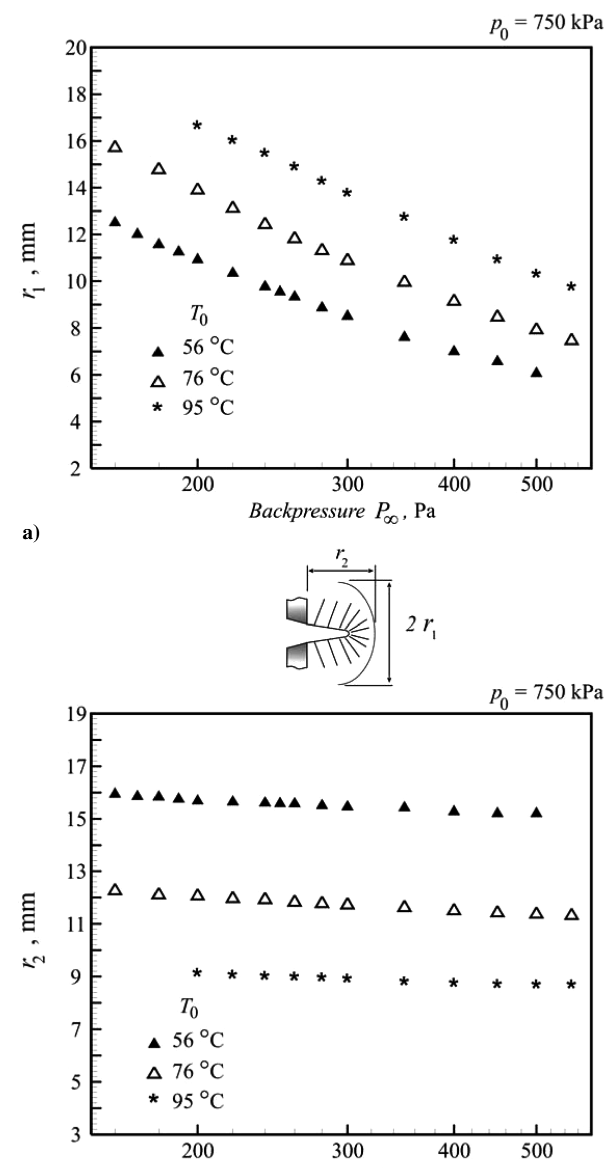

Fig. 11 Influence of shock wave maximum dimensions with temperature injection variation; numerical simulation results: a) r_1 vs backpressure and b) r_2 vs backpressure; isooctane with $P_0 = 750$ kPa for all cases.

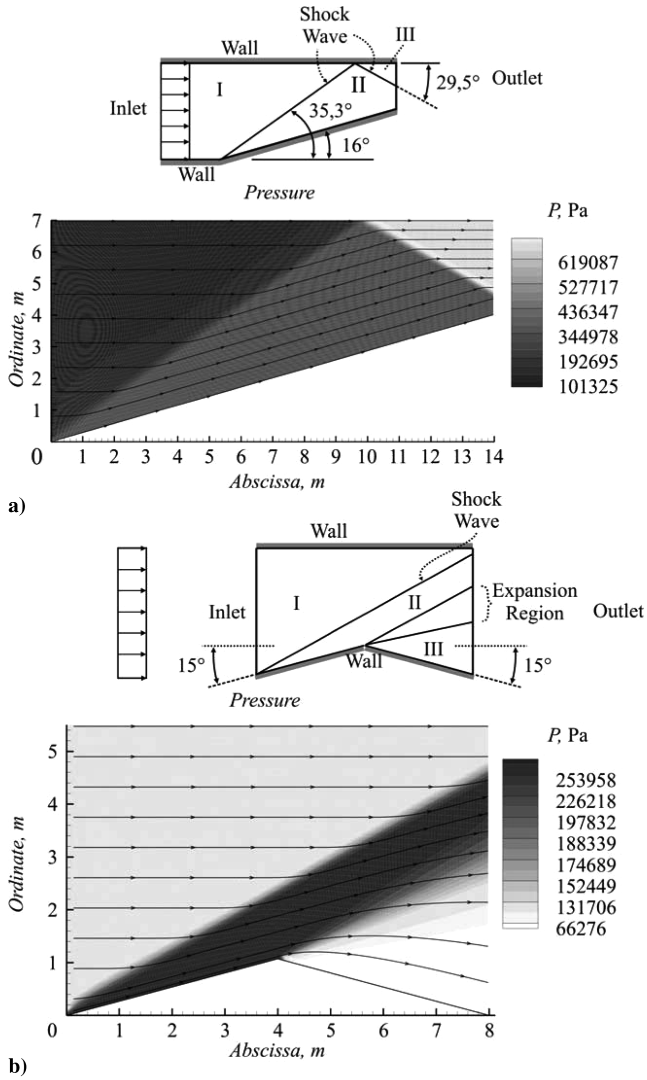

Fig. 12 Tests of the SHOWPHAST 2D code supersonic air inviscid flows [35]: a) oblique shock wave reflection case and b) oblique shock wave and Prandlt–Meyer expansion.

2) The metastable liquid core is an experimental evidence; however, the liquid evaporation ratio is unknown and was assumed as constant.

3) The boundary layer is not considered in the flow inner nozzle; its effect may produce instabilities in the nozzle exit flow [19].

4) Internal nucleation and bubble growth inside the nozzle is possible for much longer, ridged nozzles.

5) The mechanism of the evaporation front instability still remains to be completely clarified [34].

6) The constant properties inside the metastable liquid core are a model assumption without experimental evidence.

7) The homogeneous two-phase equilibrium model downstream evaporation could not be an accurate model in the cases of moderate evaporation beyond an evaporation wave.

IX. Verification, Validation and Tests of the SHOWPHAST 2D Code: Numerical Errors

The problem was solved using the numerical code SHOWPHAST 2D (shock waves with phase transition in two dimensions), developed by the first author. The FORTRAN code was tested by analytical results from inviscid supersonic air flows reported in the classic compressible flows literature [35]. The numerical errors and uncertainties found in the simulations are due [36] to discretization; artificial dissipation; incomplete iterative and grid convergence; lack of conservation of mass, momentum, and energy; computer round-off; etc. The two tested air inviscid supersonic flows were 1) oblique shock wave reflection and 2) oblique shock wave and Prandlt–Meyer expansion, which are shown in Figs. 12a and 12b, respectively.

In the first test (case a, Fig. 12a), the air inlet conditions were $P_{\mathrm{I}} = 101{,}325$ Pa, $T_{\mathrm{I}} = 288.3$ K, and $M_{\mathrm{I}} = 2.8$; the results for region 2 were $P_{\mathrm{II}} = 286{,}000$ Pa (285,736 Pa), $T_{\mathrm{II}} = 400.4$ K (400.2 K), and $M_{\mathrm{II}} = 2.061$ (2.053); and the results for region 3 were $P_{\mathrm{III}} = 663{,}448$ Pa (662,909 Pa), $T_{\mathrm{III}} = 518.2$ K (517.9 K), and $M_{\mathrm{III}} = 1.46$ (1.45). Analytical results are shown in parentheses.

In the second test (case b, Fig. 12b), the air inlet conditions were $P_{\mathrm{I}} = 101{,}325$ Pa, $T_{\mathrm{I}} = 273.15$ K, and $M_{\mathrm{I}} = 3.5$; the results for region II were $M_{\mathrm{II}} = 2.64$ (2.6); and the results for region III were $M_{\mathrm{III}} = 4.51$ (4.45). Analytical results are shown in parentheses.

The thermodynamic properties determination code was developed and tested independently.

The grid results independence, according to some authors [37], is estimated using multiple solutions (at least three) on systematically refined grids with constant refinement ratio. The refinement ratio chosen was 2; thus, the meshes tested were 55 vs 125 grid points (55 points above the metastable liquid core and 110 points for marching steps), 110 vs 250 grid points, and 220 vs 500 points. Figure 13 exemplifies the pressure distribution results for a free-vacuum-

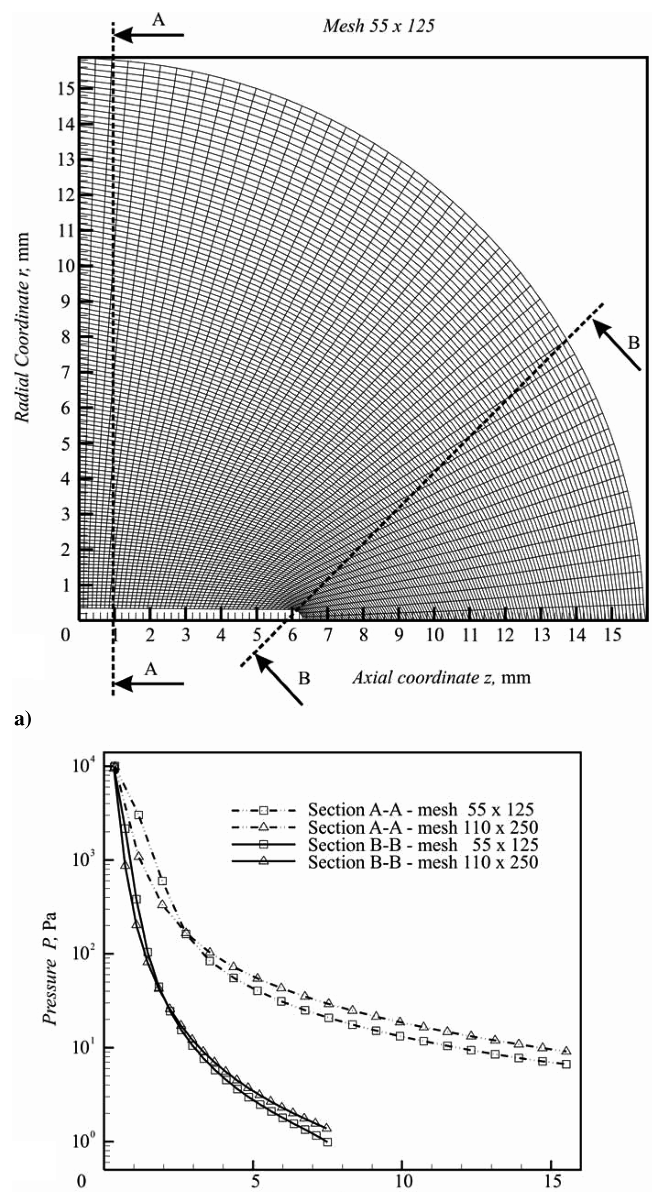

Fig. 13 Numerical grid independence tests: a) 55 vs 125 mesh grid points and b) numerical results to pressure distribution on two chosen lines for 55 vs 125 mesh grid point and 110 vs 250 mesh grid points.

expansion isooctane jet ($P_0 = 251.5$ kPa, $T_0 = 350$ K, and $P_\infty = 0$ Pa) using the three grid meshes (the 220- vs 500-points mesh has been omitted, because the values have practically been the same: 110- vs 250-density mesh). Therefore, all of the simulations have been carried out with 110 vs 250 grid points in the mesh.

X. Conclusions

Flashing phenomena can be observed in some types of phase-changing flows when highly superheated or metastable liquid jets are suddenly exposed to a low-pressure environment.

Experimental results and numerical simulations indicated that a complex compressible flow is present in such jets, just a few diameters off the nozzle exit. Based on those observations, the problem was solved numerically, using the concept of oblique evaporation waves as the phase-change mechanism from a metastable liquid state to a sonic two-phase flow (C–J condition). Next, the two-phase flow expansion continued to reach supersonic velocities, eventually terminating with a complex shock wave structure. An axisymmetric hypothesis (2-D) of the two-phase expansion model was used, which gave good results when compared with experimental data. The main shape and dimensions of the shock wave structure observed in experiments could be well captured by the numerical solution.

Acknowledgments

The authors would like to acknowledge the financial support for this project from Fundação de Amparo à Pesquisa do Estado de São Paulo (FAPESP) in Brazil. Thanks to Gabriel Angelo for helping to prepare the graphics and pictures. The second author would also like to acknowledge Conselho Nacional de Desenvolvimento Cientifico e Tecnológico (CNPQ) for personal support.

References

[1] Darby, R., "On Two-Phase Frozen Flashing Flows in Safety Relief Valves: Recommended Method and the Proper Use of the Discharge Coefficient," *Journal of Loss Prevention in the Process Industries*, Vol. 17, No. 4, July 2004, pp. 255–259.

[2] Lenzing, T., Friedel, L., Cremers, J., and Alhusein, M., "Prediction of the Maximum Full Lift Safety Valve Two-Phase Flow Capacity," *Journal of Loss Prevention in the Process Industries*, Vol. 11, No. 5, Sept. 1998, pp. 307–321.

[3] Attou, A., Bolle, L., and Seynhaeve, J. M., "Experimental Study of the Critical Flashing Flow Through a Relief Line: Evidence of the Double-Choked Flow Phenomenon," *International Journal of Multiphase Flow*, Vol. 26, June 2000, pp. 921–947.

[4] Reid, C., "Possible Mechanism for Pressurized Liquid Tank Explosion or BLEVÉs," *Science*, Vol. 23, Mar. 1979, pp. 1263–1265.

[5] Pierorazio, A. J., and Birk, A. M., "Effects of Pressure Relief Valve Behavior on 2-Phase Energy Storage in a Pressure Vessel Exposed to Fire," *Journal of Pressure Vessel Technology*, Vol. 124, No. 2, May 2002, pp. 247–252.

[6] Van den Berg, A. C., Van der Voort, M. M., Weerheijm, J., and Versloot, N. H. A., "BLEVE Blast by Expansion-Controlled Evaporation," *Process Safety Progress*, Vol. 25, No. 1, Dec. 2005, pp. 44–51.

[7] Simões-Moreira, J. R., and Bullard, C., "Pressure Drop and Flashing Mechanisms in Expansion Devices," *International Journal of Refrigeration*, Vol. 26, No. 7, Nov. 2003, pp. 840–848.

[8] Xu, S., Liang, W., and Wang, S., "Experimental Studies on Orifice Behavior and Two-Phase Flow in Flash Chamber," *Desalination*, Vol. 150, Oct. 2002, pp. 93–98.

[9] Shivayyanamath, S., and Tewari, P. K., "Simulation of Start-Up Characteristics of Multi-Stage Flash Desalination Plants," *Desalination*, Vol. 155, July 2003, pp. 277–286.

[10] Edwards, A. R., and ÓBrien, T. P., "Studies of Phenomena Connected with Depressurization of Water Reactors," *Journal of the British Nuclear Energy Society*, Vol. 9, No. 2, 1970, pp. 125–135.

[11] Forrest, C. F., and Stern, F., "Test Facilities for the Study of Thermofluid Accidents in Fusion Reactors," *Journal of Fusion Energy*, Vol. 12, No. 1–2, June 1993, pp. 95–98.

[12] Fairuzov, Y. V., "Blowdown of Pipelines Carrying Flashing Liquids," *AIChE Journal*, Vol. 44, No. 2, Feb. 1998, pp. 245–254.

[13] Pinti, D. L., and Marty, B., "Separation of Noble Gas Mixtures from Petroleum and Their Isotopic Analysis by Mass Spectrometry," *Journal of Chromatography*, Vol. 824, No. 1, Oct. 1998, pp. 109–1179).

[14] Oza, R. D., and Sinnamon, J. F., "An Experimental Analytical Study of Flash-Boiling Fuel Injection," International Congress and Exposition, Society of Automotive Engineers, Paper 830590, 1983.

[15] Gemci, T., Yakut, K., and Chigier, N., "Cavitation and Flash Boiling Atomization of Water/Acetone Binary Mixtures," *ILASS-Americas 2001: 14th Annual Conference on Liquid Atomization and Spray Systems*, Inst. for Liquid Atomization and Spray Systems (ILASS-Americas), Irvine, CA, 2001, pp. 241–246.

[16] Bolle, L., Downar-Zapolski, P., and Seynhaeve, J. M., "Experimental and Theoretical Analysis of Flashing Water Flow Through a Safety Valve," *Journal of Hazardous Materials*, Vol. 46, Apr. 1996, pp. 105–116.

[17] Bailey, J. F., "Metastable Flow of Saturated Water," *Journal of Basic Engineering*, Vol. 73, Nov. 1951, pp. 1109–1116.

[18] Lienhard, J. H., and Day, J. B., "The Breakup of Superheated Liquid Jets," *Journal of Basic Engineering*, Vol. 88, Sept. 1970, pp. 515–522.

[19] Wildgen, A., and Straub, J., "The Boiling Mechanism in Superheated Free Jets," *International Journal of Multiphase Flow*, Vol. 15, No. 2, 1989, pp. 193–207.

[20] Kitamura, Y., Morimitsu, H., and Takahashi, T., "Critical Superheated for Flashing of Superheated Liquid Jets," *Industrial and Engineering Chemistry Fundamentals*, Vol. 25, No. 2, 1986, pp. 206–211.

[21] Ramamurthi, K., and Nandakumar, K., "Disintegration of Liquid Jets from Sharp-Edged Nozzles," *Atomization and Sprays*, Vol. 4, No. 5, 1994, pp. 551–564.

[22] Reitz, R. R., "A Photographic Study of Flash-Boiling Atomization," *Aerosol Science and Technology*, Vol. 12, No. 3, 1990, pp. 561–569.

[23] Kurschat, T., Chaves, H., and Meier, G. E. A., "Complete Adiabatic Evaporation of Highly Superheated Liquid Jets," *Journal of Fluid Mechanics*, Vol. 236, 1992, pp. 43–59.

[24] Athans, R. E., "The Rapid Expansion of Near-Critical Retrograde Fluid," Ph.D. Dissertation, Rensselaer Polytechnic Inst., Troy, NY, 1995.

[25] Simões-Moreira, J. R., Vieira, M. M., and Angelo, E., "Highly Expanded Flashing Liquid Jets," *Journal of Thermophysics and Heat Transfer*, Vol. 16, No. 3, 2002, pp. 415–424.

[26] Vieira, M. M., "Estudo Experimental da Evaporação de Jatos de Iso-Octano Superaquecido," Ph.D. Dissertation, Dept. de Engenharia Mecânica, Escola Politécnica da Univ. de São Paulo, São Paulo, Brazil, 2005 (in Portuguese).

[27] Miyatake, O., and Hashimoto, T., "The Liquid Flow in Multi-Stage Flash Evaporators," *International Journal of Heat and Mass Transfer*, Vol. 35, No. 12, 1992, pp. 3245–3257.

[28] Silver, R. S., and Mitchell, J. A., "The Discharge of Saturated Water Through Nozzles," *Transactions of the North East Coast Institute of Engineers and Shipbuilders*, Vol. 62, 1951, p. 51.

[29] Pasqua, P. F., "Metastable Flow of Freon-12," *Refrigerating Engineering*, Vol. 61, Oct. 1953, pp. 1084–1089.

[30] Angelo, E., "Análise Numérica da Dinâmica da Expansão de Líquidos Superaquecidos em Evaporação Rápida," Ph.D. Dissertation, Dept. de Engenharia Mecânica, Escola Politécnica da Universidade de São Paulo, São Paulo, Brazil, 2004 (in Portuguese).

[31] Simões-Moreira, J. R., "Oblique Evaporation Waves," *Shock Waves*, Vol. 10, No. 4, 2000, pp. 229–234.

[32] Lee, B. I., and Kesler, M. G., "A Generalized Thermodynamic Correlation Based on Three-Parameter Corresponding States," *AIChE Journal*, Vol. 21, No. 3, 1975, pp. 510–527.

[33] Thompson, J. F., Soni, B. K., and Weatherill, N. P., *Handbook of Grid Generation*, CRC Press, Boca Raton, FL, 1999.

[34] Simões-Moreira, J. R., and Shepherd, J. E., "Evaporation Waves in Superheated Dodecane," *Journal of Fluid Mechanics*, Vol. 382, 1999, pp. 63–68.

[35] Anderson, J. D., *Modern Compressible Flow: With Historical Perspective*, McGraw–Hill, New York, 1990.

[36] Stern, F., Wilson, R. V., Coleman, H. W., and Paterson, E. G., "Comprehensive Approach to Verification and Validation of CFD Simulations, Part 1: Methodology and Procedures," *Journal of Fluids Engineering*, Vol. 123, Dec. 2001, pp. 793–802.

[37] Wilson, R. V., Stern, F., Coleman, H. W., and Paterson, E. G., "Comprehensive Approach to Verification and Validation of CFD Simulations, Part 2: Application for RANS Simulation of a Cargo/Container Ship," *Journal of Fluids Engineering*, Vol. 123, Dec. 2001, pp. 803–809.